C.P. No. 870

MINISTRY OF AVIATION

AERONAUTICAL RESEARCH COUNCIL

CURRENT PAPERS

Procedure for the Determination of Cascade Characteristics

By

J. A. P. Stoddart and D. Gardner

LONDON: HER MAJESTY'S STATIONERY OFFICE

1966

SIX SHILLINGS NET

C.P. No.870

November, 1964

A Procedure for the Determination of Cascade Characteristics

- By -
J. A. P. Stoddart and D. Gardner

SUMMARY

This note presents an approximate procedure for the theoretical calculation of the aerodynamic characteristics of an infinite cascade of arbitrary aerofoils. The effects of subcritical compressibility and viscosity are included and some experimental comparisons are presented.

The procedure has been programmed in Alphacode for use on DEUCE.

CONTENTS

1./

Replaces B.A.C. Report No. Ae 204 - A.R.C.27 181.

1. Introduction

The design of axial flow turbomachinery is at present carried out with the use of semi-empirical design curves, such as those published by N.G.T.E., and in many cases these are satisfactory. However, it is becoming more and more desirable to limit the weight of such machinery whilst retaining the performance and this can be done using high stagger blading not covered by existing charts.

In devising a procedure to calculate blade characteristics, by what is termed the direct method, a three-dimensional viscous calculation is not yet possible, and, in any case, would be extremely complex.

If it is assumed that useful results can be obtained by two-dimensional calculations at, say, the mean blade height, a procedure can be devised using existing approximate cascade theories.

This note outlines such a method and enables a designer to look at extremes of stagger and solidity not normally covered by existing charts as well as the more normal values of these quantities. It should be noted that the methods used are only approximate but should, at least, give correct trends.

2. Outline of Theory

The method requires a knowledge of the blade section; stagger and spacing together with the inflow conditions, in order to estimate the effects of compressibility and viscosity on the blade (i.e., outflow conditions, losses, operating range, Mach number characteristics etc.).

The procedure consists of the extension of an inviscid incompressible solution[1] to subcritical viscous flow. The effect of compressibility on the incompressible potential solution is obtained by an extension to cascade flow of the well known Prandtl-Glauert transformation for isolated aerofoils[2]. Boundary-layer development on the blades is calculated by standard methods[3,4,5] using Mager's compressibility transformation[6]. The effect of the boundary layer on the potential flow is taken from Ref. 7.

2.1 Schlichting's incompressible potential solution[1]

This is a singularity method whereby the flow through an infinite cascade is represented by the superimposition of:

1. A translational flow representing the throughflow.

2. A continuous source distribution representing the thickness distribution.

3. A continuous vortex distribution representing the camber distribution and lift.

The calculation procedure is simplified by placing the source and vortex distributions on the chordline, rather than on the mean camber line. The method is thereby restricted to small values of maximum camber height and maximum thickness (say 10%). This is ample for most compressor cascades but not for strongly cambered turbine cascades.

Given/

Given the stagger angle λ^* (Fig. 1), blade solidity c^*/s^*, air inlet angle α^*_{id} and the blade profile one can calculate the pressure distribution around the contour, the air outlet angle α^*_{2id} the blade lift coefficient C^*_{Lid} and other inviscid parameters of lesser interest.

Schlichting's method has been programmed in DEUCE α-code at the Mechanical Engineering Laboratory Whetstone and is summarised in Refs. 8, 9 and 10.

Schlichting's theory contains further simplifying assumptions which restrict the type of blade profile which can be accurately calculated. The blade must have a cusped trailing edge to avoid a T.E. singularity and have distributions of thickness and camber which can be represented by 3 term trigonometric series. The method of Ref. 8 contains a smoothing process whereby a given profile is approximated by a '3 term' profile for which an accurate solution is obtained and differences between the profiles are concentrated near the trailing edge. It is not thought that these restrictions are serious.

Schlichting's method has also been programmed for representation by a 15 term trigonometric series[19] but the computation time is excessive for the added accuracy.

Fig. 2 shows some comparisons of experimental and theoretical pressure distributions taken from Ref. 7. High-stagger high-solidity compressor cascades have been selected as these are of current interest. Agreement is seen to be satisfactory provided that:

1. Boundary-layer separation is not extensive : compare Figs. 2a and 2b.

2. The solidity is not so great that the semi-linearised theory begins to break down : compare Figs. 2c and 2d.

The theory is expected to yield useful results in cascade geometries which do not have combinations of high camber, thickness and solidity.

2.2 Potential flow compressibility transformation[2]

The method is based on an extension of the Prandtl-Glauert transformation for a single aerofoil: see Fig. 3.

Putting $\Omega = \sqrt{(1 - M_\infty^2)}$ where M_∞ is the vector mean Mach number, the relevant results of the transformation are:

$$\tan \alpha^*_{\infty id} = \frac{1}{\Omega} \tan \alpha_{\infty id}$$

$$\lambda^* - \alpha^*_{\infty id} = \lambda - \alpha_{\infty id}$$

$$\alpha^*_{1id} - \alpha^*_{\infty id} = \alpha_{1id} - \alpha_{\infty id}$$

and similarly for α_{2id}

C*/S*

$$C^*/S^* = (C/S)\sec \alpha_{\infty id}/\sqrt{(\Omega^2 + \tan^2\alpha_{\infty id})}$$

where * denotes the equivalent incompressible geometry.

The transformation is non-dimensional and in Fig. 3, C^* has been chosen to be equal to C.

It is seen that for a given configuration in compressible flow at Mach number M_∞, the equivalent geometry at $M_\infty = 0$ has higher stagger, solidity and fluid angles. The blade profiles are unchanged since the boundary conditions of the problem are satisfied on the blade chord and not on the profile. The method may not be used if the blade camber, thickness and solidity become too great: this is consistent with the restrictions in para. 2.1.

The pressure distributions around the actual and equivalent geometries are related by:

$$C_{p\infty id}(\lambda, C/S, \alpha_{\infty id}, M_\infty) = \frac{1}{\Omega} C^*_{p\infty id}(\lambda^*, C^*/S^*, \alpha^*_{\infty id}).$$

Similar expressions hold for C_{Lid} and C_{Mid}. The linearisation involved in the transformation requires that fluid angles relative to the blade chord (at large distances from the cascade) remain unchanged and that deflection angles are small and thus independent of Mach number.

Fig. 4 shows comparisons of experimental and theoretical velocity distributions taken from Ref. 11. These theoretical results were obtained by the method of Ref. 1 in conjunction with a transformation which differs slightly from that of Ref. 2. Agreement is quite acceptable in these cases considering the relatively high solidity and thick blade profile.

2.3 Calculation of the boundary layer

Boundary-layer development is calculated by conventional theory and the methods are summarised in Refs. 3, 4, 5 and 6. The boundary-layer compressibility transformation used[6] differs from the potential flow compressibility transformation[2] in that a change in length scale occurs. The transformation of Ref. 2 alters the planform of the cascade without reference to physical size and the transformation of Ref. 6 is assumed to alter the physical size and Reynolds number without changing the planform.

2.3.1 Estimation of transition position

A great area of uncertainty lies in the position of boundary-layer transition. At the Reynolds numbers under investigation (approx. $3 \cdot 10^5$ based on the blade chord) it is expected that laminar flow will exist for 10 to 20% of the chord. Some evidence is available on the value of momentum defect thickness Reynolds number at transition in incompressible flow ($R^*_{\theta^*_t}$) and is shown in Fig. 5. The correlating function is inflow Reynolds number although $R^*_{\theta^*_t}$ will also depend upon the degree of freestream turbulence, the

roughness/

roughness and curvature of the surface and the shape of the applied pressure distribution. Ref. 12 suggests that a value $R^*_{\theta^*_t} = 250$ is a reasonable estimate for turbomachinery due to the high level of turbulence present. Ref. 13 presents observed values of $R^*_{\theta^*_t}$ for cascades using blades of the N.G.T.E. C.4 section with 30° and 40° of circular arc camber. Ref. 14 presents transition lines observed by dust deposits on a 4-bladed fan and on a two-dimensional cascade blade of the same section and at the same inflow Reynolds number and incidence. The variation of inflow Reynolds number in Fig. 5 for the fan corresponds to different stations along the blade. Large three-dimensional effects can be seen on the fan data due, presumably, to a stabilising effect of the radial pressure gradient.

The bulk of the data falls within the range,

$$150 < R^*_{\theta^*_t} < 300$$

and it is proposed to use a constant value of $R^*_{\theta^*_t} = 250$ for cascade calculations unless boundary layers are artificially 'tripped'.

2.3.2 Estimation of separation point

The method of Ref. 3 predicts laminar separation at a transformed shape parameter $H^* = 3{\cdot}55$ and turbulent separation is normally supposed to occur in the range $1{\cdot}8 < H^* < 2{\cdot}6$. Ref. 15 presents a two parameter correlation of laminar and turbulent separation positions. This suggests that if boundary-layer separation is to be treated as a one parameter occurrence then the values

$$H^*_{sp} = 3{\cdot}5 - 3{\cdot}6 \quad \text{laminar}$$

$$H^*_{sp} = 2{\cdot}4 - 2{\cdot}6 \quad \text{turbulent}$$

should suffice. The actual values of H^* at separation are not too critical since the growth of H^* is normally very rapid.

An independent check on separation positions predicted by conventional boundary-layer theory can be made by Stratford's methods for laminar and turbulent flow[16]. These methods postulate that a boundary layer in a pressure rise may be divided into two regions,

(1) an outer layer in which the pressure rise merely lowers the dynamic lead profile, and shear losses being almost identical to flat plate flow

(2) an inner layer in which the inertia forces are so small that the velocity profile is distorted by the pressure rise until the pressure gradient is balanced by the transverse shear gradient.

The theory is developed so that the flow development length to separation can be found from the pressure rise and pressure gradient at separation. The pertinent results of the theory are summarised in Ref. 17.

2.4/

2.4 Effect of viscosity on cascade flow[7]

The growth of boundary-layer displacement thickness on the blade alters the effective thickness and camber distributions and can be represented by small changes in the source and vortex distribution used in Ref. 1. The induced velocities around the blades are changed by a small amount hence altering the inflow, outflow and vector mean air angles. The inviscid pressure distribution obtained by the methods of Refs. 1 and 2 is assumed to apply to viscous flow through the cascade at slightly different air angles. The total head loss behind the cascade is obtained from the momentum defect thickness at the trailing edge by a method similar in result to the well known Squire and Young equation for isolated aerofoils. A further small correction to the outflow angle is deduced on account of the reduced total lead in the outflow.

Allowance is made for the existence of small amounts of boundary-layer separation at the rear of the blade. This is an important part of the theory since many cascade configurations have maximum L/D when the rear of the blade has some separation.

The method is derived for incompressible flow and the solution is performed in the transformed plane and the results transformed back to compressible flow.

3. DEUCE Programmes and Procedure

3.1 Summary of available programmes

Schlichting's method for the calculation of inviscid, incompressible flow through a cascade of arbitrary aerofoils has been programmed in Alphacode for DEUCE in three parts.

(1) The calculation of the influence coefficients which are a function only of stagger and solidity (Warton Prog. No. 561/A and Ref. 8).

(2) Blade profile smoothing and calculation of thickness and camber gradients at specified points along the blade (Warton Prog. No. 561/B and Ref. 9).

(3) The calculation of potential pressure coefficients (based on outlet conditions) at specified points on the blade, the overall lift coefficient and outflow angle in potential flow. This programme uses the results of (1) and (2) above with a specified inflow angle (Warton Prog. No. 561/C and Ref. 10).

In order to use these programmes when the flow through the cascade is compressible, it is necessary to find the equivalent incompressible geometry and air angles (Woolards transformation). (Warton α-code Prog. No. 144/0 and Ref. 2.) The incompressible pressure coefficient output from Prog. 561/C is converted to vector mean reference then to compressible flow by Woolard's transformation and finally to a Mach number distribution (Warton α-code Prog. No. 144/4). Pitching moment about the L.E. is calculated at this stage.

This completes the inviscid calculation.

Boundary-layer/

Boundary-layer development is calculated in the transformed plane using the external potential pressure distribution (Warton α-code Prog. No. 144/5). The associated losses and influence of the boundary layer on the potential flow are also calculated in the transformed plane (Warton α-code Prog. No. 144/6). If required, Stratford's method (Warton α-code Prog. No. 144/7) may be used to confirm or otherwise the existence of separations predicted by Prog. 144/5. Finally transformed aerodynamic characteristics of the cascade are converted to compressible flow. This part of the calculation has not been programmed.

An auxiliary programme (Warton α-code Prog. No. 144) is available for the calculation of the ordinates of N.G.T.E. circular arc and parabolic arc camber lines.

3.2 Computation of outflow angle in compressible flow

In order to apply Woolard's transformation to compressible flow[2] it is necessary to know the vector mean air angle α_∞ and the vector mean Mach number M_∞. In general the inlet conditions will be known together with the mass flow rate per unit area. If a reasonable guess can be made of some outflow conditions, say α_2 using the deviation rule Ref. 18, an iterative procedure can be set up to converge on the correct α_2 and hence vector mean conditions.

Given the cascade geometry and inflow conditions, a reasonable range of α_2 is selected and used in Prog. 144/0. This programme produces a range of transformed geometries and flow angles as the vector mean conditions vary with α_2, α_1, being constant.

The corresponding variations of α^*_∞ and α^*_1, produced by this programme may be plotted against the values of α_2 (Fig. 6). Programmes 561/A and 561/C are used with the transformed geometries and inflow angles to produce a second variation of α^*_∞ (and α^*_2).

The value of α_2 at which the variations of α^*_∞ coincide is the correct value within the theoretical limitations. Due to the approximations made in the theory of Ref. 2, the final value of α^*_2 may not be entirely consistent with α_2. This restriction is not severe unless large deflections are required at high Mach number.

3.3 Application to incompressible flow

If the flow through the cascade can be considered incompressible, Prog. No. 144/0 and the procedure in para. 3.2 may be omitted. However, consistent realistic values of 'incompressible' M_∞, $R(x)/x$ and a_s/ν_s must be specified for Progs. 144/4, 5 and 7 in order to get the Reynolds number scale correct and to ensure that the transformations operate correctly in the limit of small M_∞.

3.4/

3.4 Calculation time

(a) Incompressible flow

Approximately 30 min for the first inflow angle and 15 min per succeeding inflow angle.

(b) Compressible flow

Approximately 60 min for the first inflow angle and 25 min for each succeeding inflow angle.

A block diagram of the programmes available is shown in Fig. 7.

4. Comparison with Experiment

Figs. 8 and 9 present comparisons of the proposed theory with incompressible experimental results of Ref. 7. Boundary-layer flow is fully turbulent and calculations are performed entirely from theory. Ref. 7 presents a comprehensive survey of experimental characteristics for cascades of NACA 8410 and 0010 blade sections. The geometry of Fig. 8 is representative of high-stagger, high-solidity blading with limited separation and should provide a fair test of the validity of the theory for incompressible flow. The geometry of Fig. 9 is less extreme but has more extensive separation and may lie outside the limits of the theory.

4.1 Pressure distributions Figs. 8B and 9B

The comparison of Fig. 8B is seen to be good except downstream of the separation point. The effects of a separated region are not included in the pressure distribution calculation. The relatively small amount of separation in Fig. 8 does not appear to have affected the upstream pressures to any great extent.

The agreement of Fig. 9B is poor for two reasons. Extensive boundary-layer separation has strongly influenced upstream pressures and there appears to be a local separation near the nose.

4.2 Position of separation

Fig. 8A suggests that the observed separation point may be predicted when the theoretical H^* is in the range 1·8 to 2·0 provided that separation is not extensive. The difference between these values and those given in para. 3.3 may be due to the difference between the experimental and theoretical pressure distributions. Fig. 9A shows that the observed separation point cannot be predicted from the theoretical pressure distribution when the separation becomes extensive. Separation can be called extensive when it covers more than 20% of the blade chord. Predictions of separation by Stratford's method appear to be slightly pessimistic. Agreement could, no doubt, be improved by use of the experimental pressure distribution.

4.3 Force, deflection characteristics and working range

Figs. 8C to 8F, 9C to 9F indicate that the variations of C_L, C_D, ζ_ν $\Delta V/U$ and ε are predicted satisfactorily provided that separation is not extensive.

From/

From Figs. 8 and 9 crude criteria can be found to predict the upper and lower limits of the working range. The upper limit to the working range is largely governed by trailing-edge separation and arbitrarily, the upper limit is chosen at the point where theoretical separation covers the last 20% of the upper blade surface, i.e., the C_L where $H^* = 1{\cdot}9$ (say) at $x/c = 0{\cdot}8$. This limit is shown in Figs. 8 and 9 and crudely corresponds to the point where the experimental C_D begins to depart markedly from the mid-range value. The lower limit is probably governed by leading-edge separation, especially on highly cambered profiles, and at low Reynolds numbers it will be a laminar separation. A lower limit to the working range can be obtained on this basis by say, Stratford's work[17].

Also presented in Figs. 8 and 9, are the calculations of Ref. 7. Apart from Figs. 8C to 8F, the discrepancies between the present calculation and the calculations of Ref. 7 can be attributed to the differences between hand and automatic calculation. The discrepancies in Figs. 8C to 8F are probably due to a systematic error in that particular set of calculations in Ref. 7 since the present calculations give much better agreement with experiment. Ref. 7 presents a large number of comparisons of theory with experiment which indicate that theory and experiment are in good agreement provided that separation is not extensive.

No comparisons have been made in compressible flow as the present writers are not aware of compressible cascade measurements as comprehensive as the incompressible measurements of Ref. 7.

5. Conclusions and Recommendations

Since the theory used in this Note leans heavily on linearisation, good predictions cannot be expected for geometries which have combinations of large camber, thick blades and high solidity or for geometries which have local supersonic flow or extensive regions of separation. Certainly, if such combinations are avoided, adequate predictions are obtained in incompressible flow. Whether the same is true in compressible flow cannot be decided until further comparisons are available. If such calculations confirm the approximations made, there seems no reason why the procedure should not be programmed for a very fast computer and used to produce design charts for extreme geometries.

NOTATION/

NOTATION

x,y	Distance along and normal to blade (ft)
c	Blade chord (ft)
s	Blade pitch (ft)
U,V,W	Axial, tangential and resultant velocity (ft/sec)
M	Mach number
$\Omega = \sqrt{(1 - M^2)}$	
α	Air angle (deg)
$\beta = \alpha + 90$ (deg)	
λ	Blade stagger (deg)
ϕ_{LE}, ϕ_{TE}	Angle between chord and camber line at leading and trailing edges (deg)
i	Camberline incidence, $i = \alpha - \lambda - \phi_{LE}$ (deg)
d	Deviation angle $d = \alpha_2 - \lambda + \phi_{TE}$ (deg)
ε	Deflection angle $\varepsilon = \alpha_1 - \alpha_2$ (deg)
ρ	Fluid density (slugs/cu ft)
P,p	Total and static pressure (lb/sq ft)
ν	Kinematic viscosity (ft^2/sec)
$\frac{\Delta V}{U}$	Cascade deflection coefficient $\frac{\Delta V}{U} = \tan \alpha_1 - \tan \alpha_2$
ζ_ν	Cascade loss coefficient $\zeta_\nu = \frac{P_1 - P_2}{\frac{1}{2}\rho_1 U_1^2}$
C_L, C_D	Lift and drag coefficients per unit span

$$C_L = \frac{\text{lift/unit span}}{\frac{1}{2}\rho_{\infty\infty} W^2_{\infty\infty} c} \qquad C_D = \frac{\text{drag/unit span}}{\frac{1}{2}\rho_{\infty\infty} W^2_{\infty\infty} c}$$

C_P	Pressure coefficient $C_p = \frac{p - p_{ref}}{\frac{1}{2}\rho_{ref} W^2_{ref}}$

θ/

θ Boundary-layer momentum defect thickness

$$\theta = \int_0^\infty \frac{\rho W}{\rho_e W_e}\left(1 - \frac{W}{W_e}\right) dy$$

H Boundary-layer form parameter

$$H = \int_0^\infty \left(1 - \frac{\rho W}{\rho_e W_e}\right) d\left(\frac{y}{\theta}\right)$$

$R_\theta = \frac{W_e \theta}{\nu_e}$ Momentum defect thickness Reynolds number

SUFFICES

1 Inflow conditions, i.e., far upstream of cascade

2 Outflow conditions, i.e., far downstream of cascade

∞ Vector mean conditions defined by Fig. 1

t Position of boundary-layer transition

e Conditions at edge of boundary layer

id Potential flow

sp Position of boundary-layer separation

SUPERSCRIPT

* Denotes incompressible function defined by the compressibility transformations

---

REFERENCES/

REFERENCES

No.	Author(s)	Title, etc.
1	H. Schlichting	Calculation of the frictionless incompressible flow for a given two-dimensional cascade (Direct problem). NACA Misc. 128, 1958.
2	H. W. Woolard	A note on subsonic compressible flow about airfoils in a cascade. J. Aeronaut. Sci. Vol.17, 1950, pp.379-381.
3	N. Curle	The laminar boundary-layer equations. O.U.P. 1962.
4	E. C. Maskell	Approximate calculation of the turbulent boundary layer in two-dimensional incompressible flow. A.R.C.14 654, November, 1951.
5	H. Schlichting	Boundary-layer theory. McGraw Hill, 4th Edition, 1960.
6	A. Mager	Transformation of the compressible turbulent boundary layer. J. Aeronaut. Sci. Vol.25, 1958, pp.305-311.
7	L. Speidel and N. Scholz	Investigations into the flow losses of cascades (In German). V.D.I. Forschungsheft 464, 1957.
8	E. C. Brew	Singularities method of hydrofoil cascade computation. E.E.C. Ltd. Whetstone M.E.L. Report W/M (4A), p.40, 1959.
9	G. A. Pennington	Data smoothing and differentiation for Schlichting's calculations. E.E.C. Ltd. Whetstone M.E.L. Report W/M (4A), p.152, 1963.
10	E. C. Brew	Calculation of the aerodynamic parameters of an hydrofoil in cascade. E.E.C. Ltd. Whetstone M.E.L. Report W/M (4A), p.41, 1959.
11	E. G. Feindt and H. Schlichting	Calculation of the frictionless flow for a given cascade at high subsonic speeds (In German). Z.A.M.P. Vol.IXb, 1958, pp.274-284.
12	A. W. Goldstein and A. Mager	Attainable circulation about airfoils in cascade. NACA Report 953, 1950.

13/

No.	Author(s)	Title, etc.
13	D. J. K. Stuart	Analysis of Reynolds number effects in fluid flow through two-dimensional cascades. A.R.C. R. & M.2920, July, 1952.
14	E. T. Hignett and M. M. Gibson	Surface flow patterns as visualised by dust deposits on the blades of a fan. J. R. Ae. Soc. Vol.67, 1963, pp.589-594.
15	V. A. Sandborn and S. J. Kline	Flow models in boundary-layer stall inception. J. Basic Eng. Vol.83, Series D, 1961.
16	B. S. Stratford	Prediction of separation of the turbulent boundary layer. J.F. M. Vol.5, 1959, pp.1-16.
17	D. Gardner	Prediction of boundary-layer separation in compressible flow by Stratford's methods. Warton α-code Prog. No. 144/7.
18	J. H. Horlock	Axial flow compressors. Butterworth 1958.
19	D. Pollard and J. Wordsworth	A comparison of two methods for predicting the potential flow about arbitrary aerofoils in cascade. A.R.C. C.P.618, June, 1962.

HD

D 74172/1/125875 K4 9/66 XL

CASCADE NOTATION

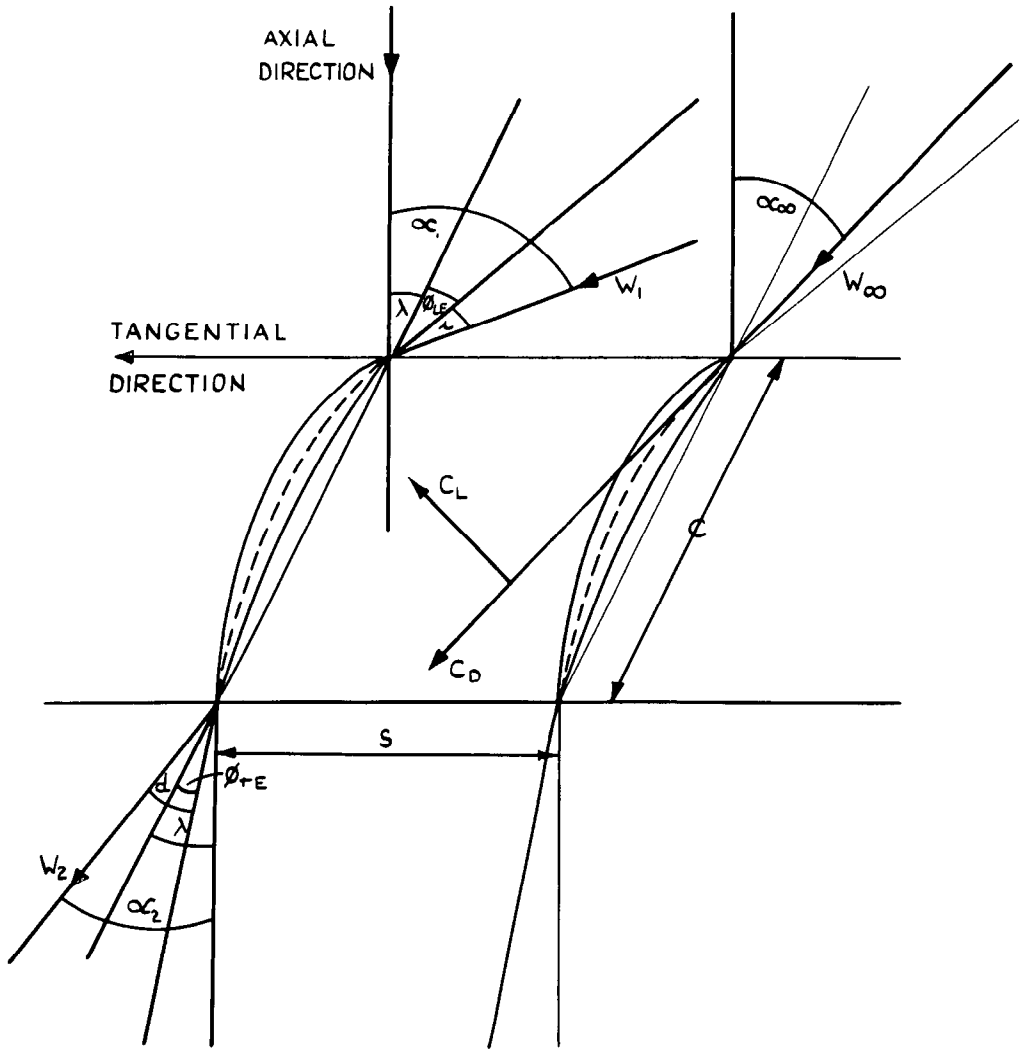

VELOCITY DIAGRAM

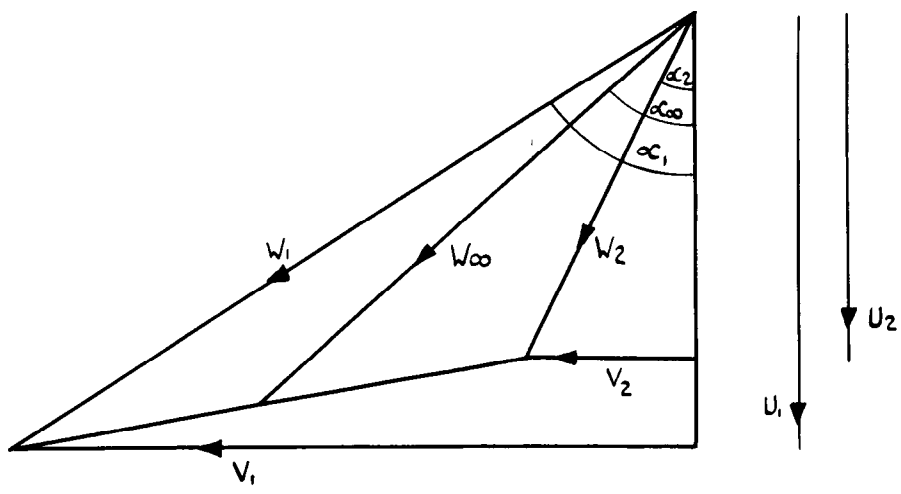

COMPARISON OF THEORETICAL & EXPERIMENTAL PRESSURE DISTRIBUTIONS SP DENOTES OBSERVED POSITION OF SEPARATION FIG.2

NACA 8410 $\lambda = 60°$

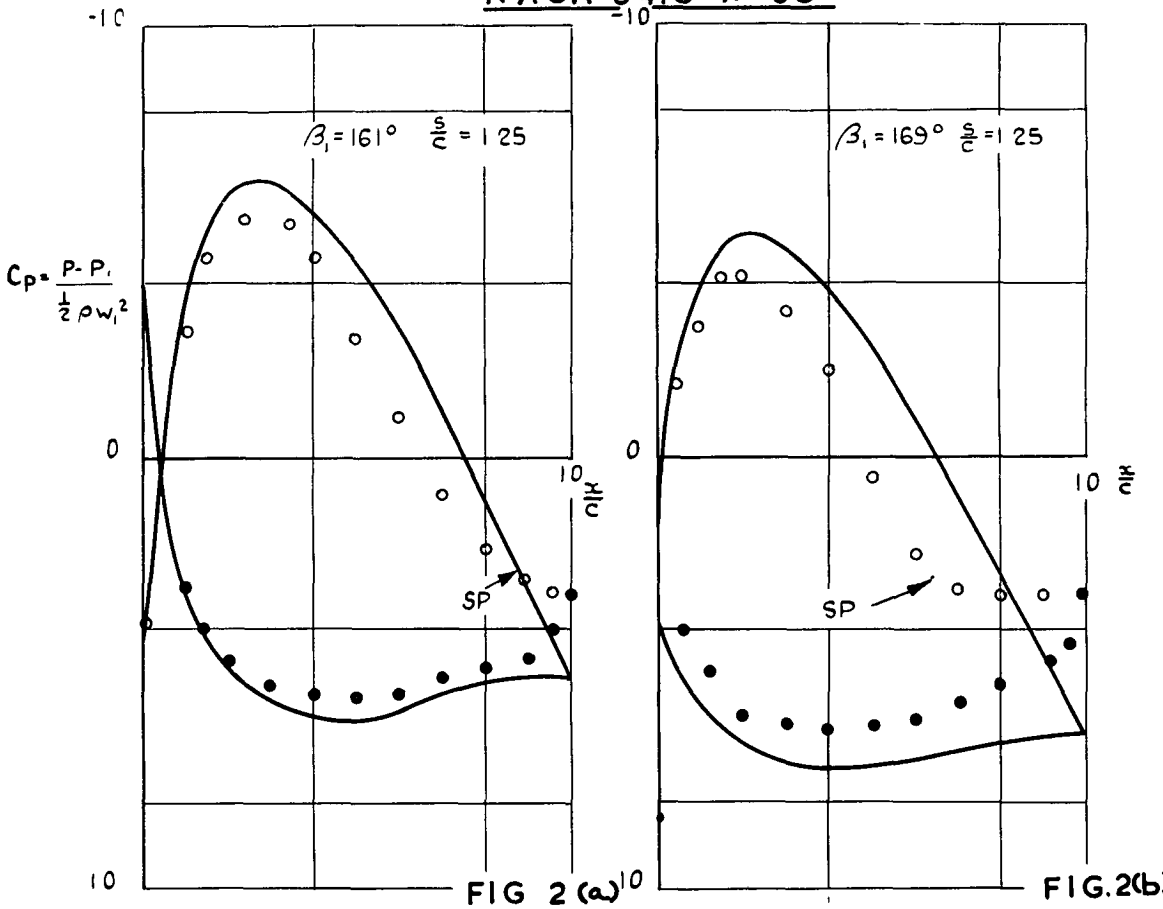

NACA 0010 $\lambda = 60°$

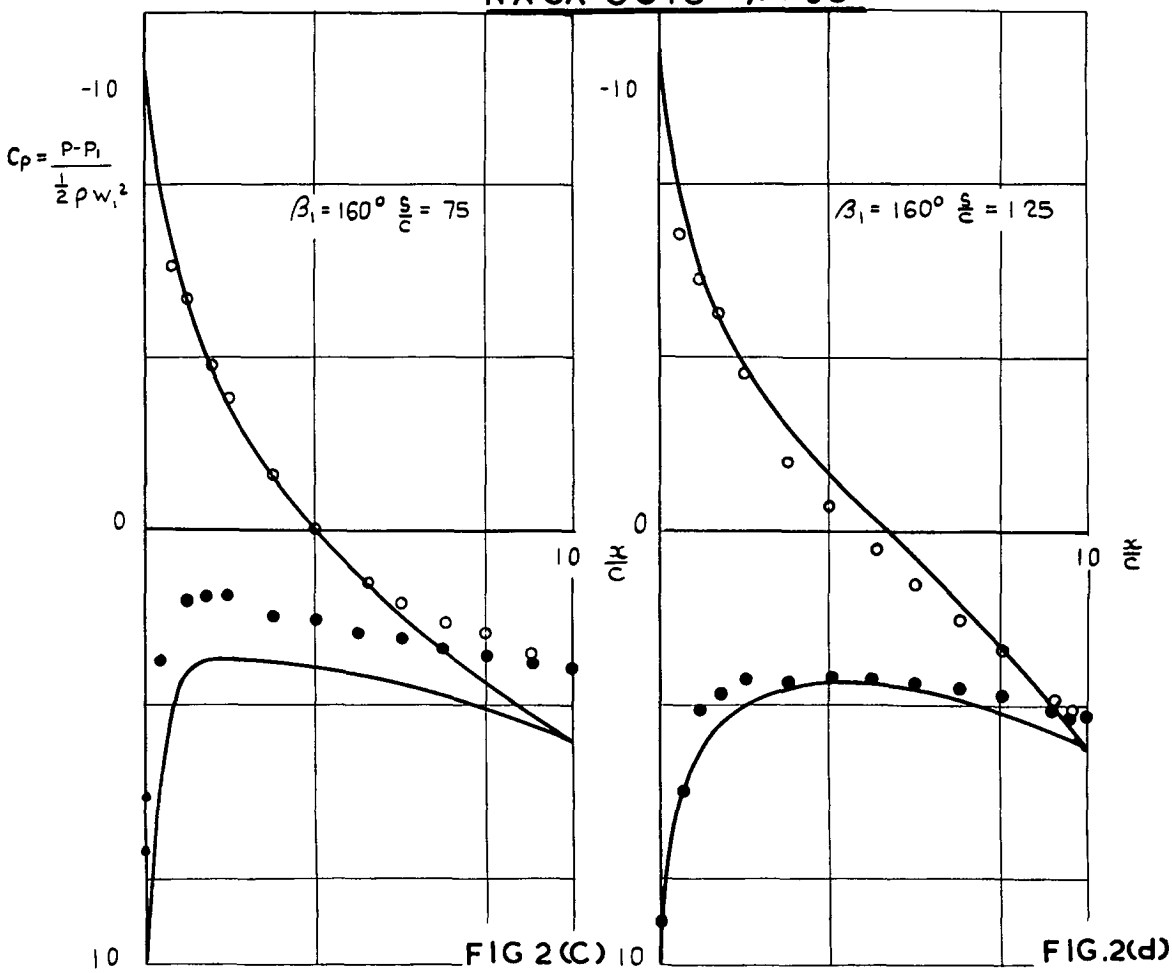

—— THEORY EXPERIMENT { o UPPER SURFACE, ● LOWER SURFACE

TRANSFORMATION OF THE POTENTIAL FLOW

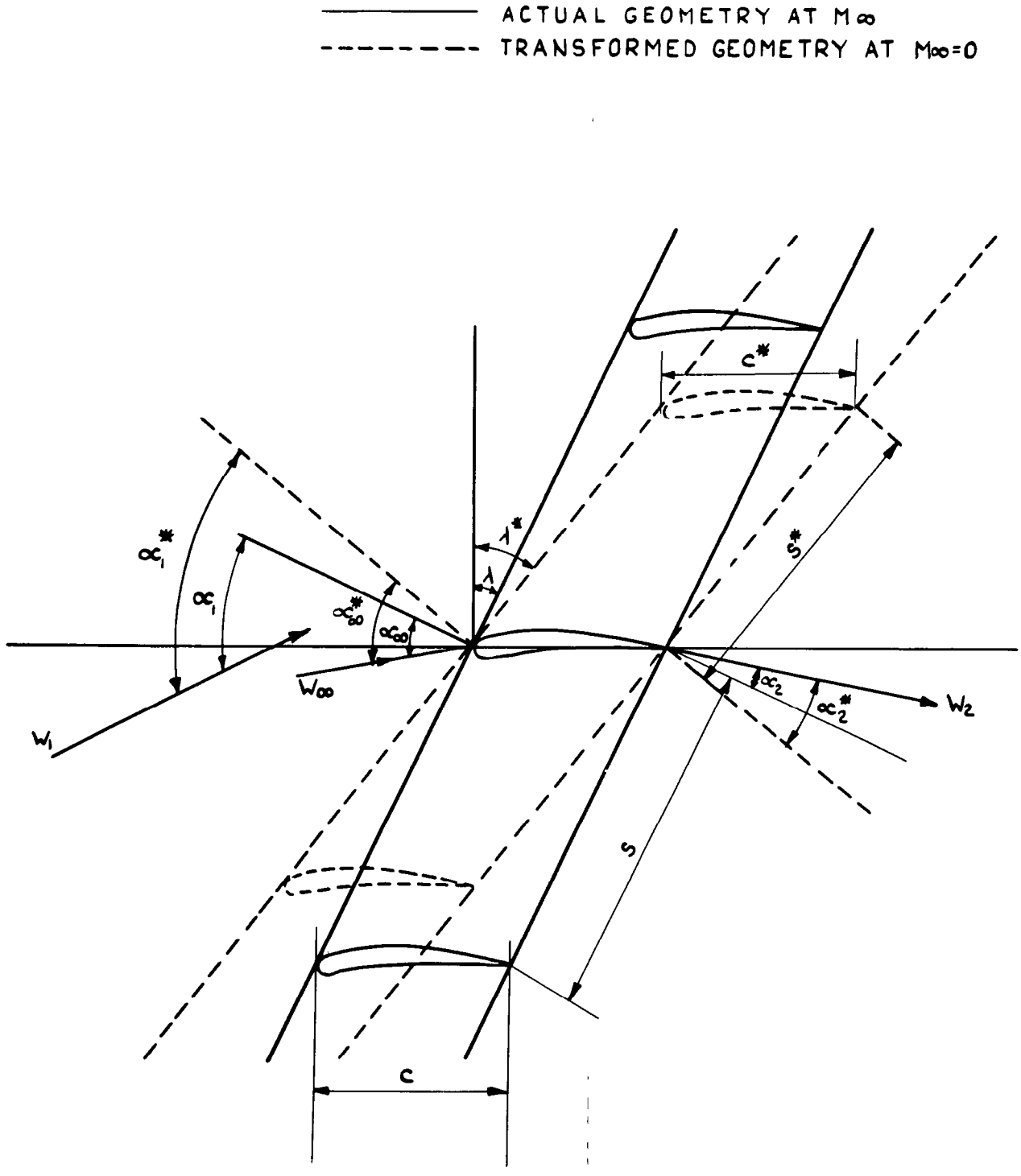

COMPARISON OF THEORETICAL & EXPERIMENTAL VELOCITY RATIO FOR AN UNSTAGGERED CASCADE OF NACA 0010 PROFILES AT A PITCH/CHORD RATIO OF 1·0. FIG. 4

$M_1 = \frac{W_1}{C_1} = 65$ $\quad Re = \frac{W_1 c}{\nu} = 3 \times 10^5$

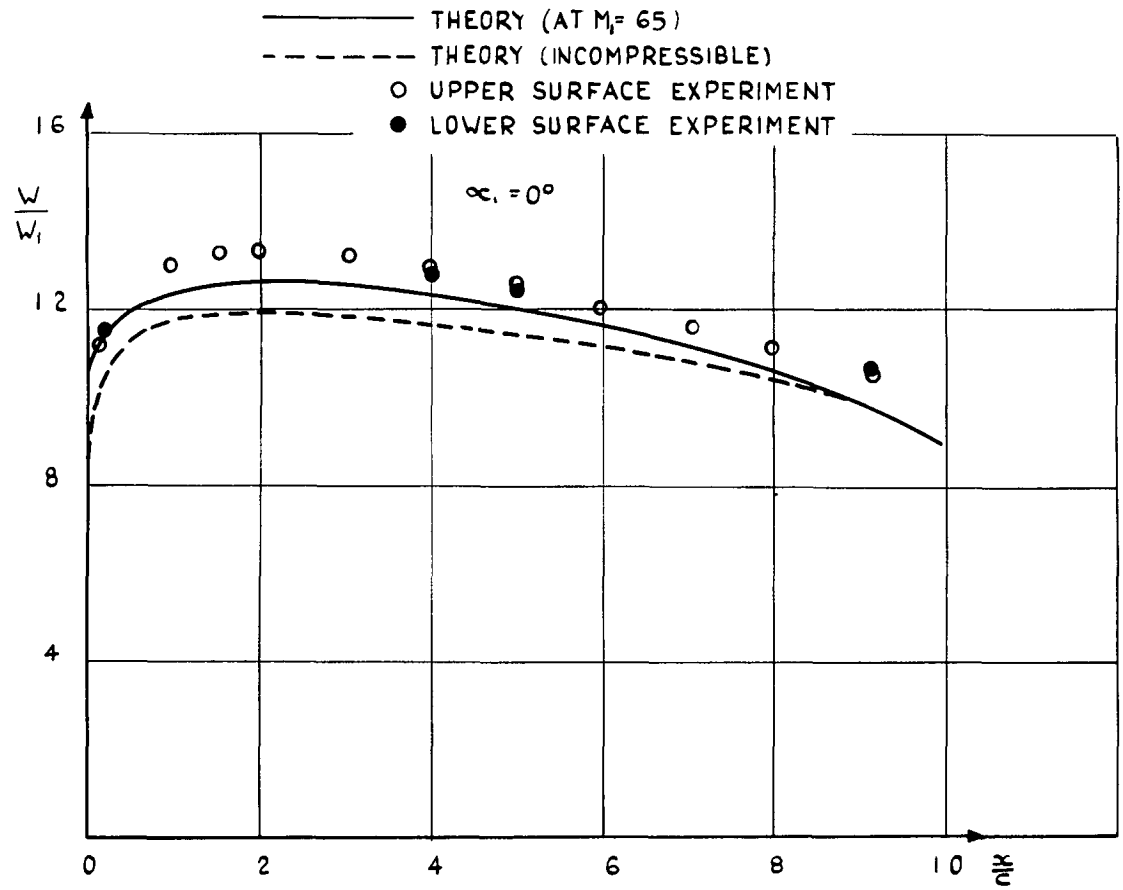

FIG. 4(a)

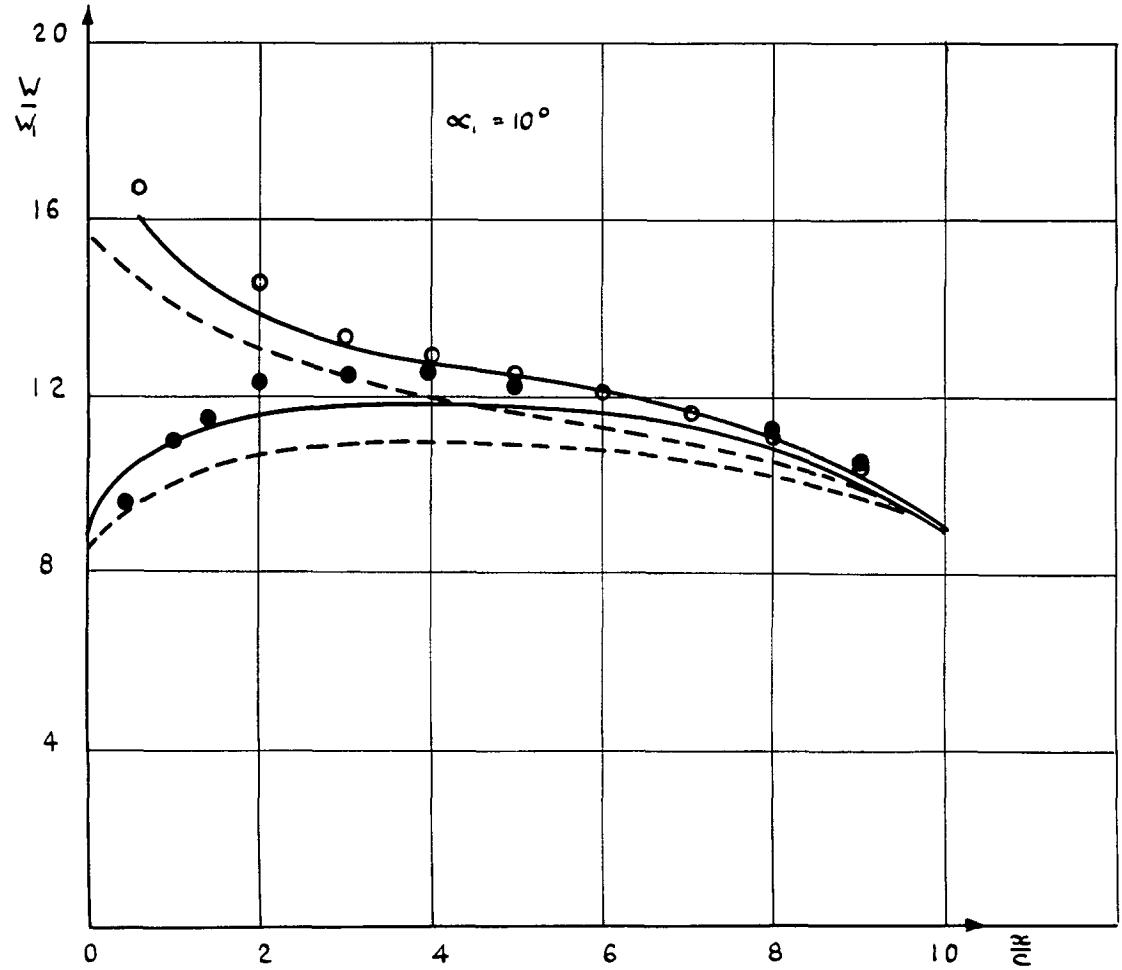

FIG. 4(b)

CORRELATION OF MOMENTUM DEFECT THICKNESS REYNOLDS NUMBER AT TRANSITION

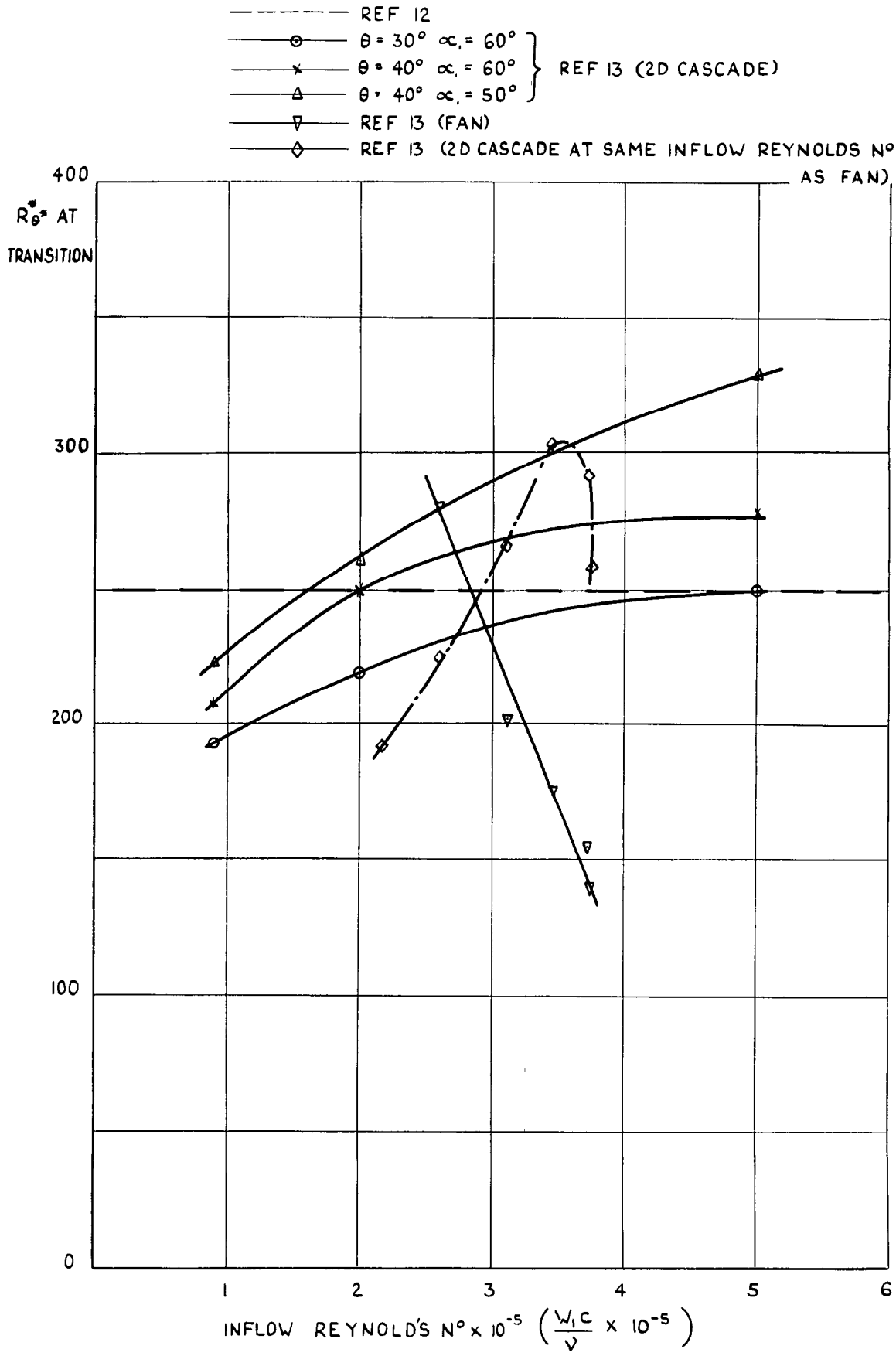

FIG. 6

ITERATIVE PROCEDURE FOR CALCULATING VECTOR MEAN CONDITIONS IN COMPRESSIBLE FLOW

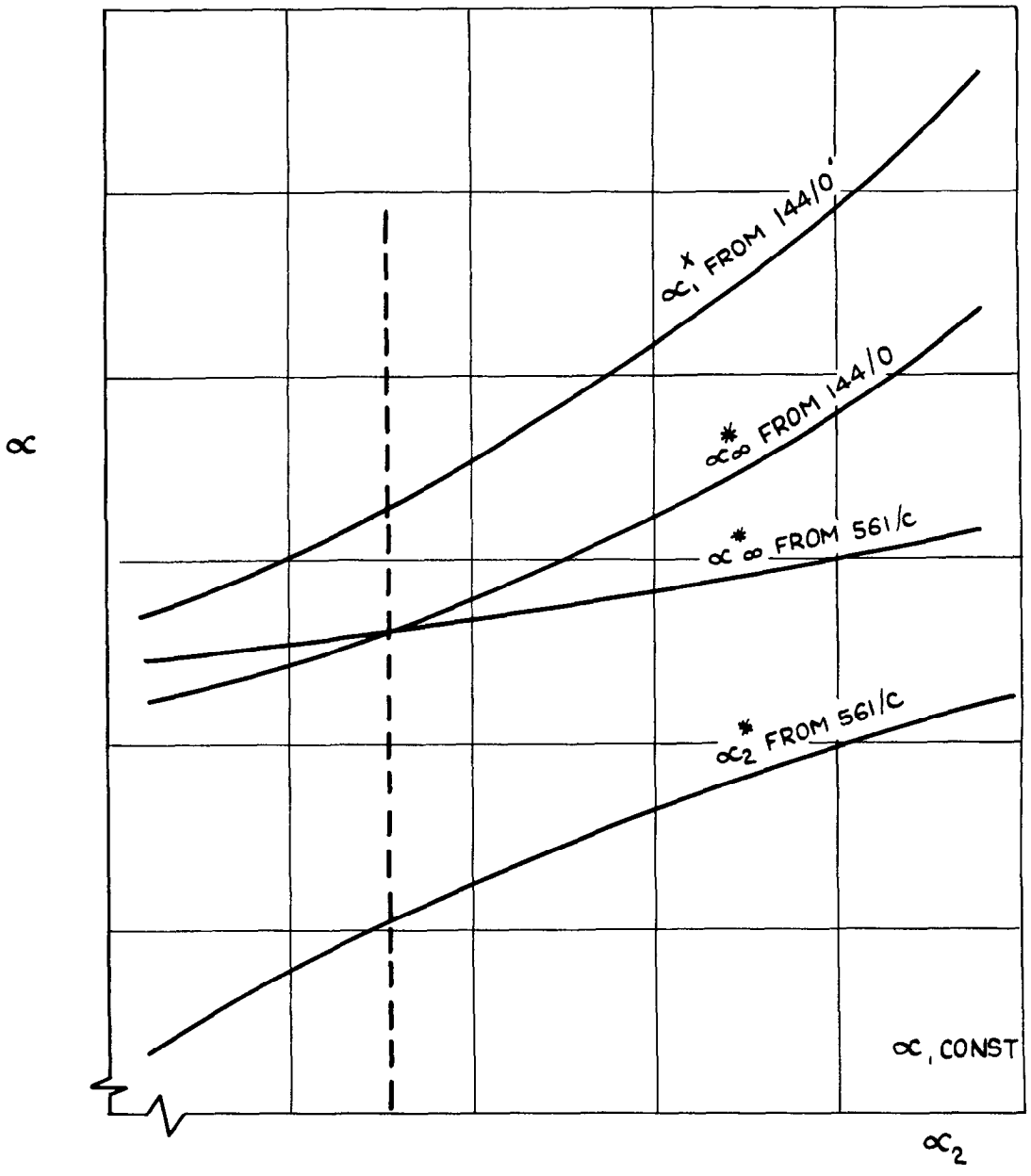

FIG 7

PROGRAMME LINKS

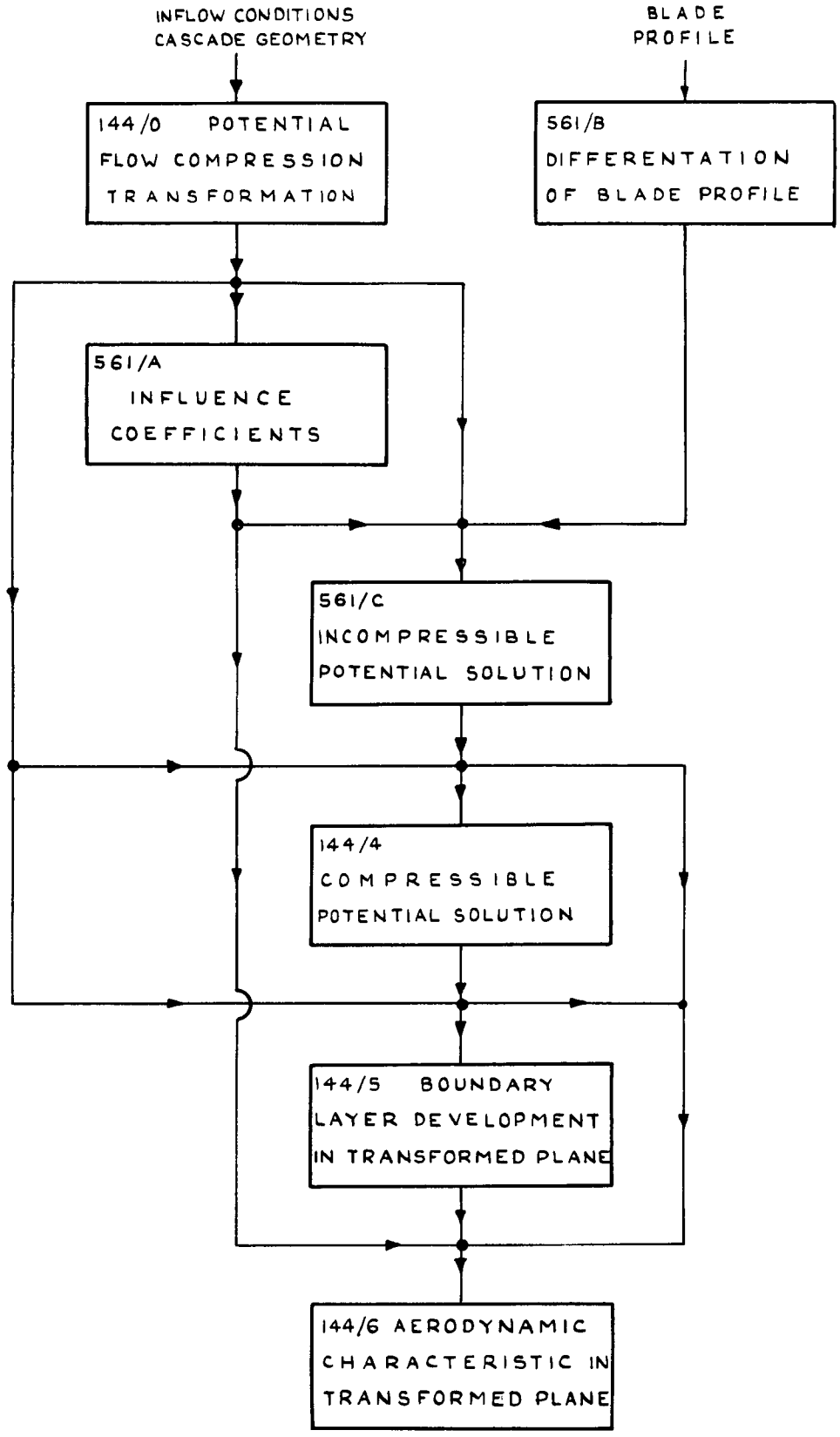

THE PRINCIPAL FUNCTION OF EACH PROGRAMME IS INDICATED
DETAILS OF THE LINKS CAN BE FOUND IN THE PROGRAMME WRITE UP

COMPARISON OF EXPERIMENTAL AND THEORETICAL CASCADE CHARACTERISTICS

FIG 8

NACA 8410 PROFILE $\lambda = 60°$ $s/c = 1.0$ $Re = 9.7 \times 10^5$

MEASURED AND ESTIMATED SEPARATION POINTS

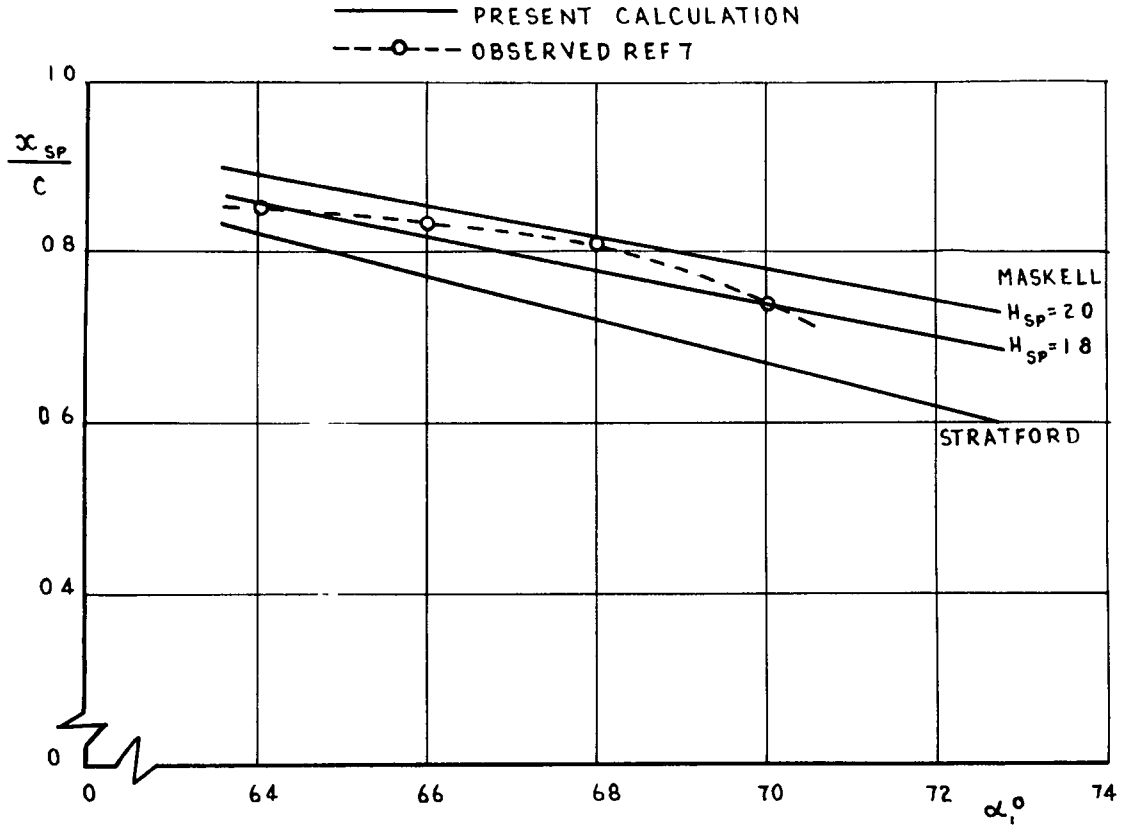

FIG. 8A

MEASURED AND ESTIMATED PRESSURE DISTRIBUTIONS

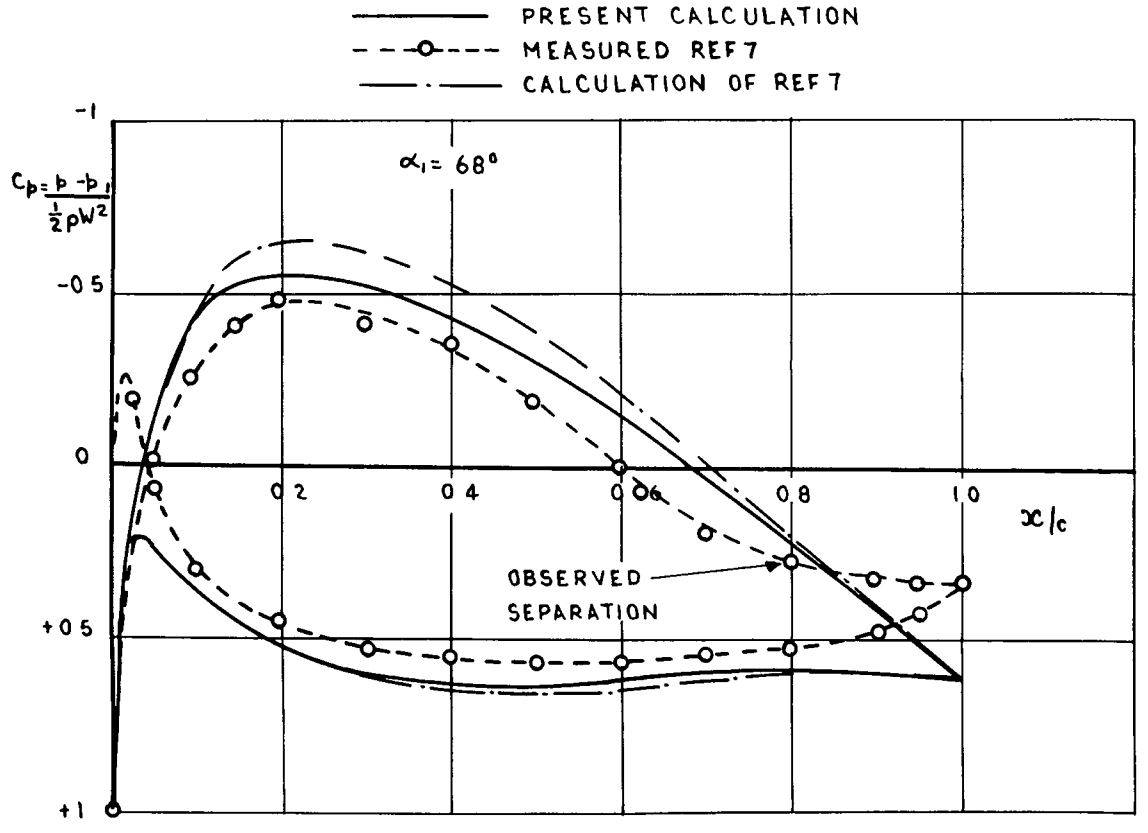

FIG 8B

FIG 8 CONT

MEASURED AND ESTIMATED LIFT DRAG POLAR.

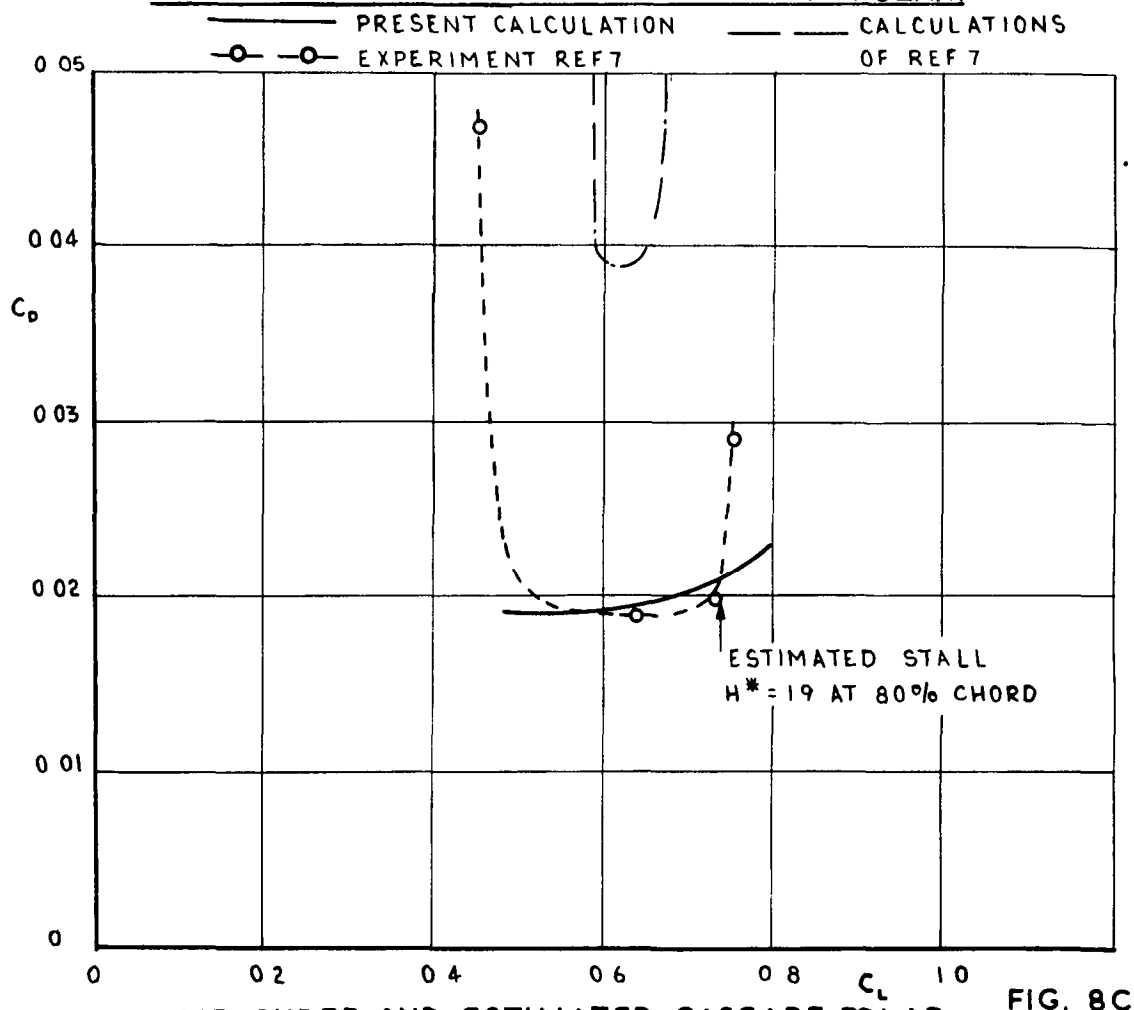

FIG. 8C

MEASURED AND ESTIMATED CASCADE POLAR.

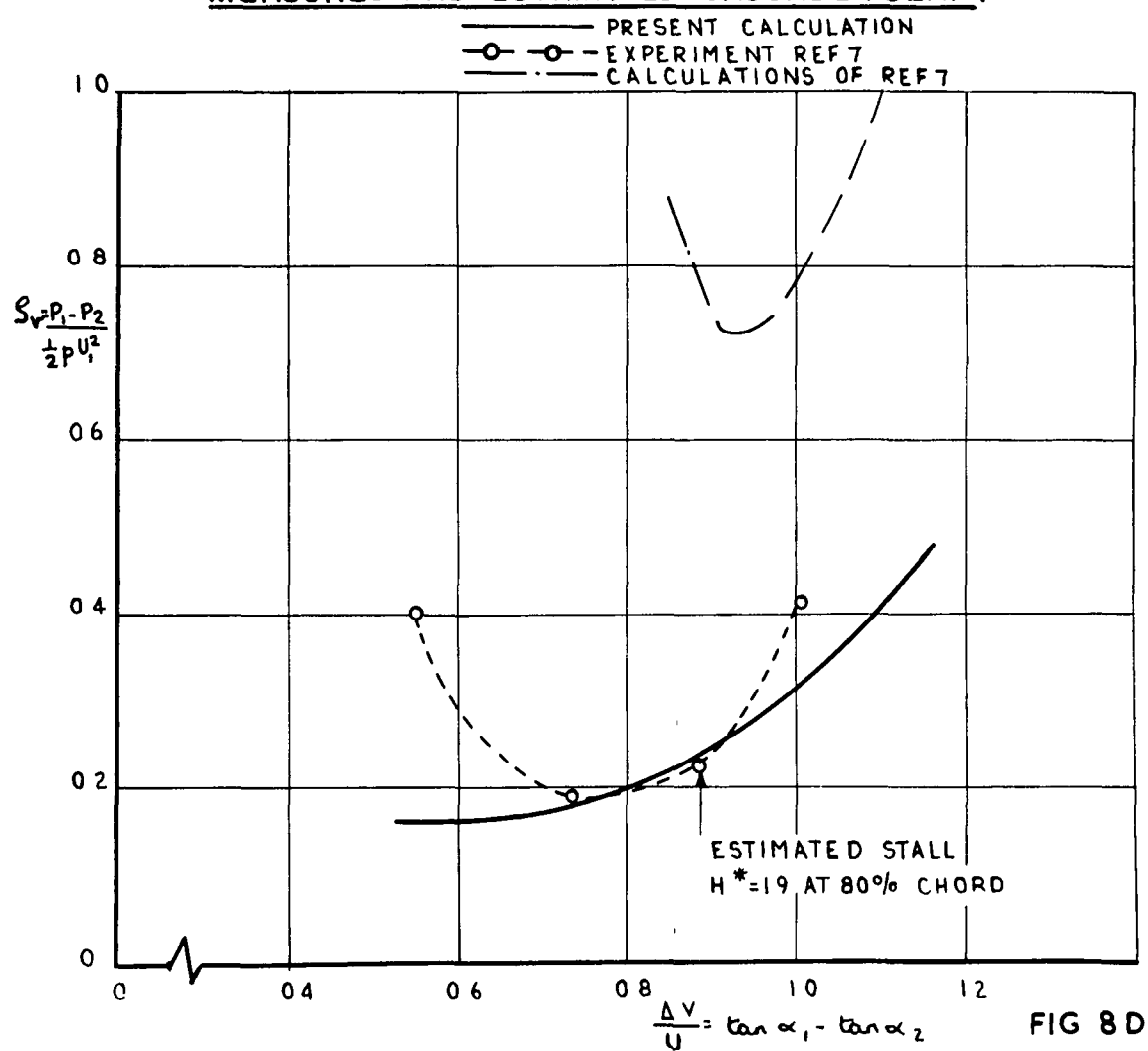

FIG 8D

FIG 8CONT.

EXPERIMENTAL AND CALCULATED LIFT/DRAG RATIO

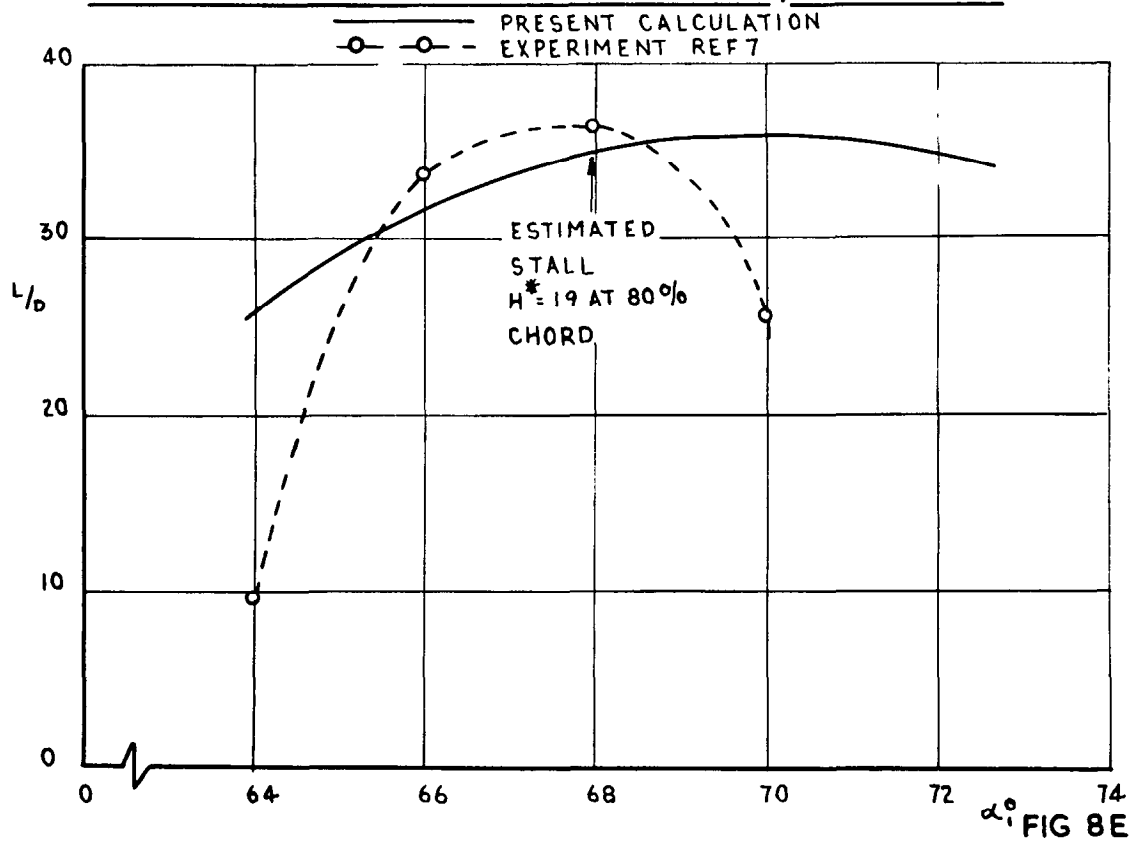

FIG 8E

EXPERIMENTAL AND CALCULATED DEFLECTION

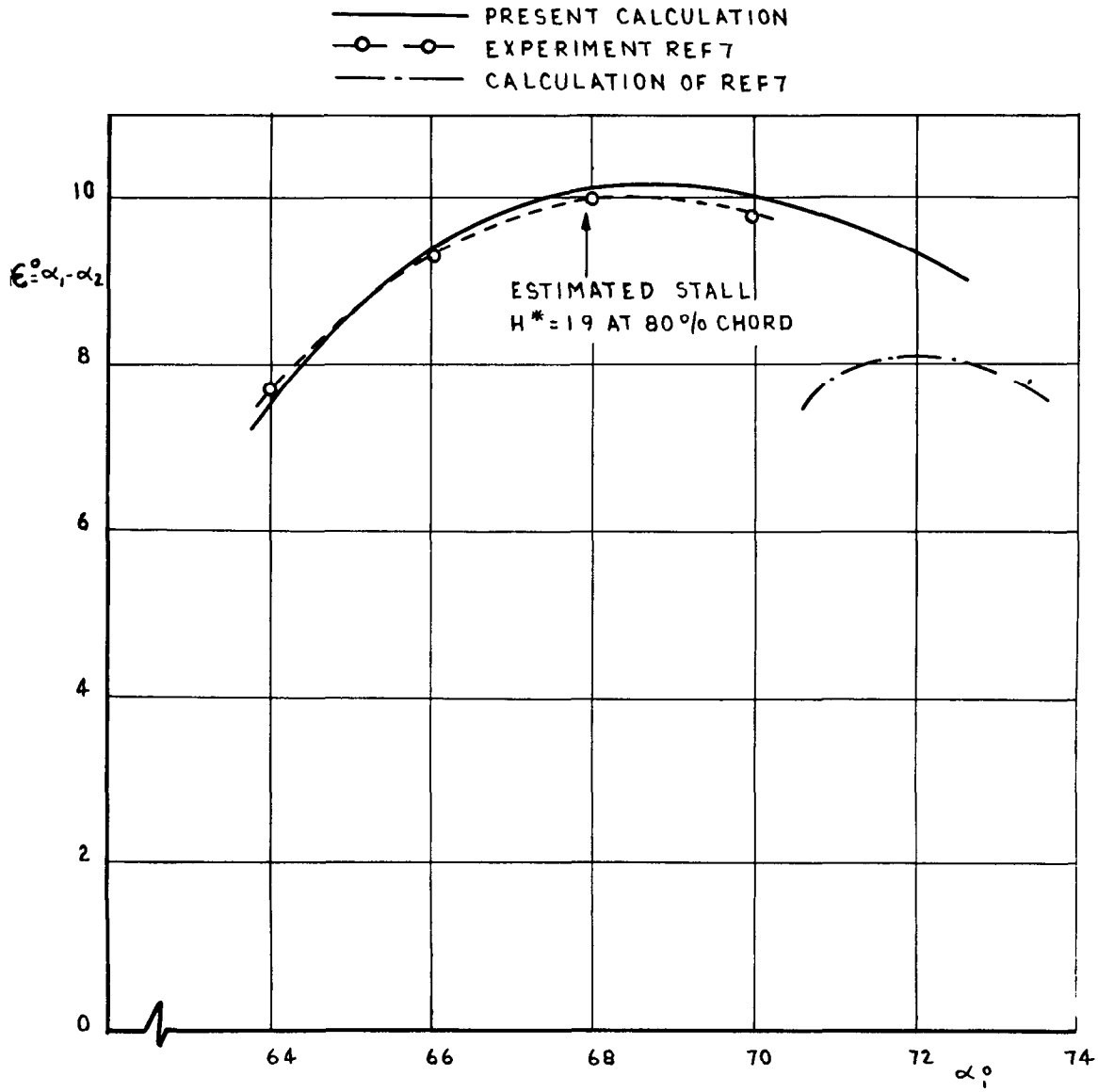

FIG 8F

FIG9

COMPARISON OF EXPERIMENTAL AND THEORETICAL CASCADE CHARACTERISTICS

NACA 8410 PROFILE $\lambda = 30°$ $s/c = 1.25$ $Re = 9.7\,10^5$

MEASURED AND ESTIMATED SEPARATION POINTS

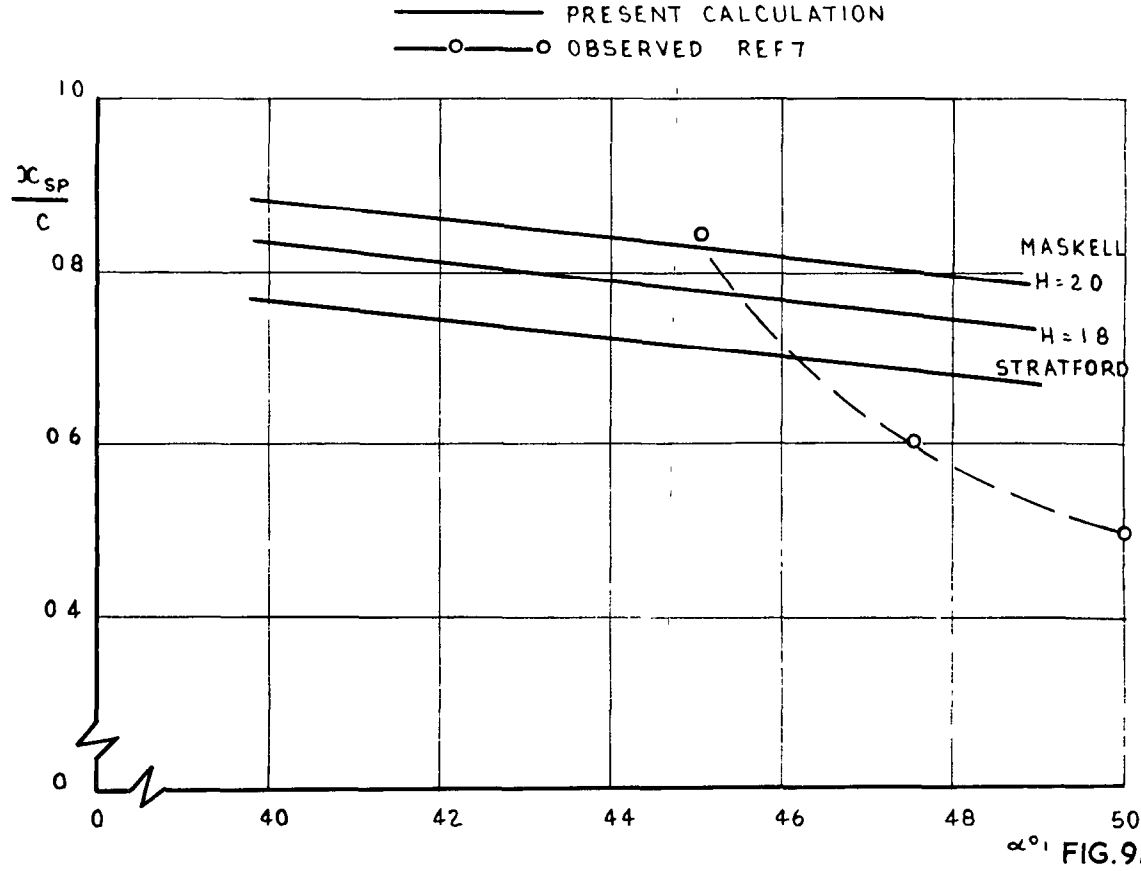

FIG.9A

MEASURED AND ESTIMATED PRESSURE DISTRIBUTIONS.

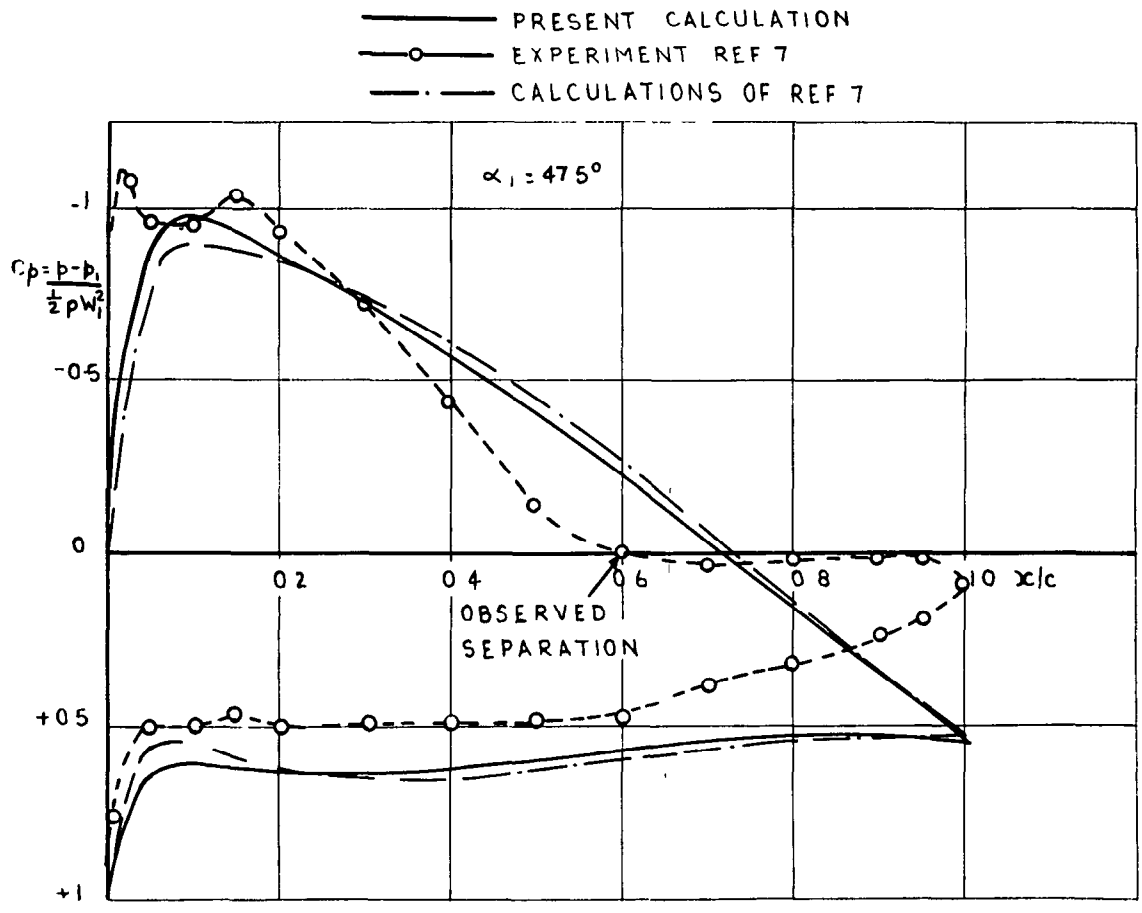

FIG 9B

MEASURED AND ESTIMATED LIFT DRAG POLAR.

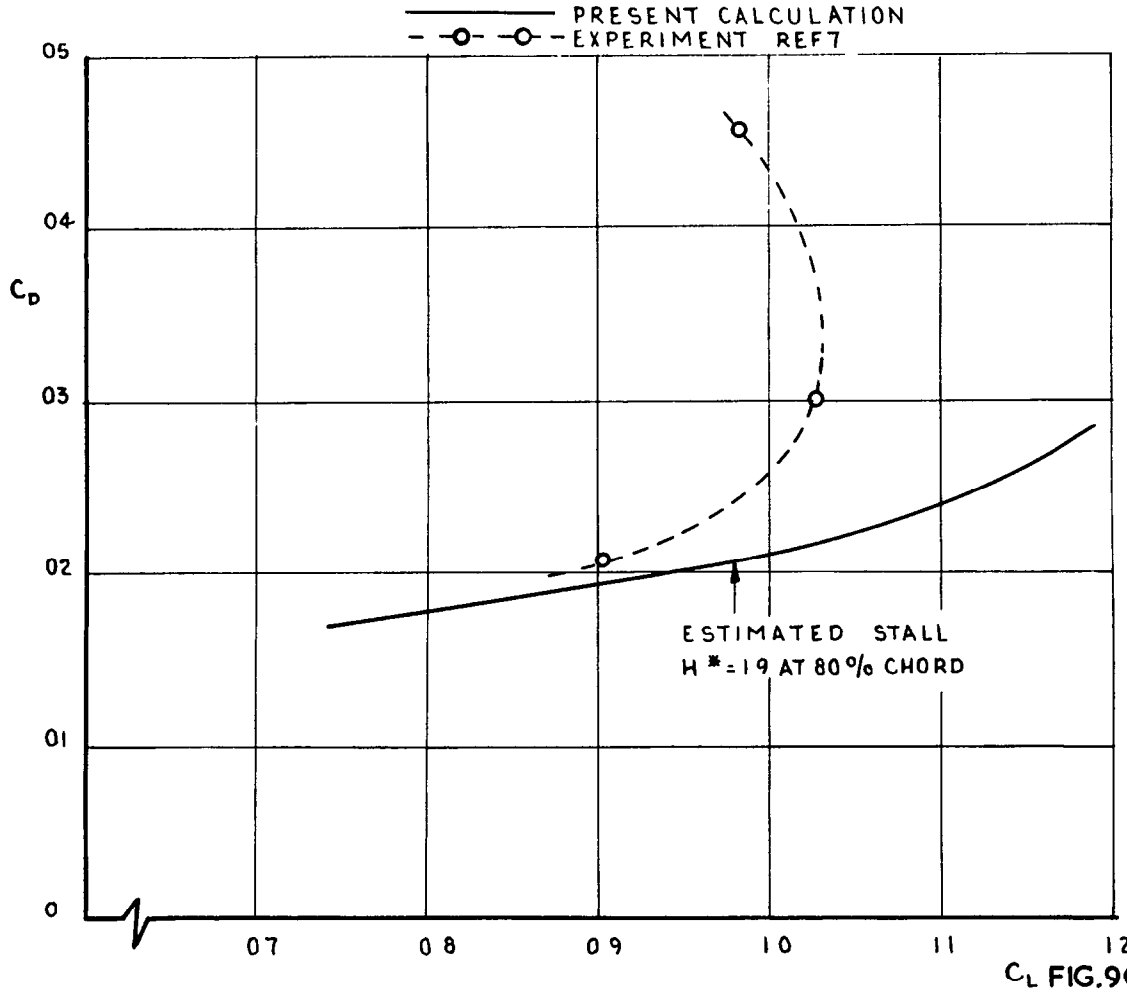

FIG. 9C

MEASURED AND ESTIMATED CASCADE POLAR

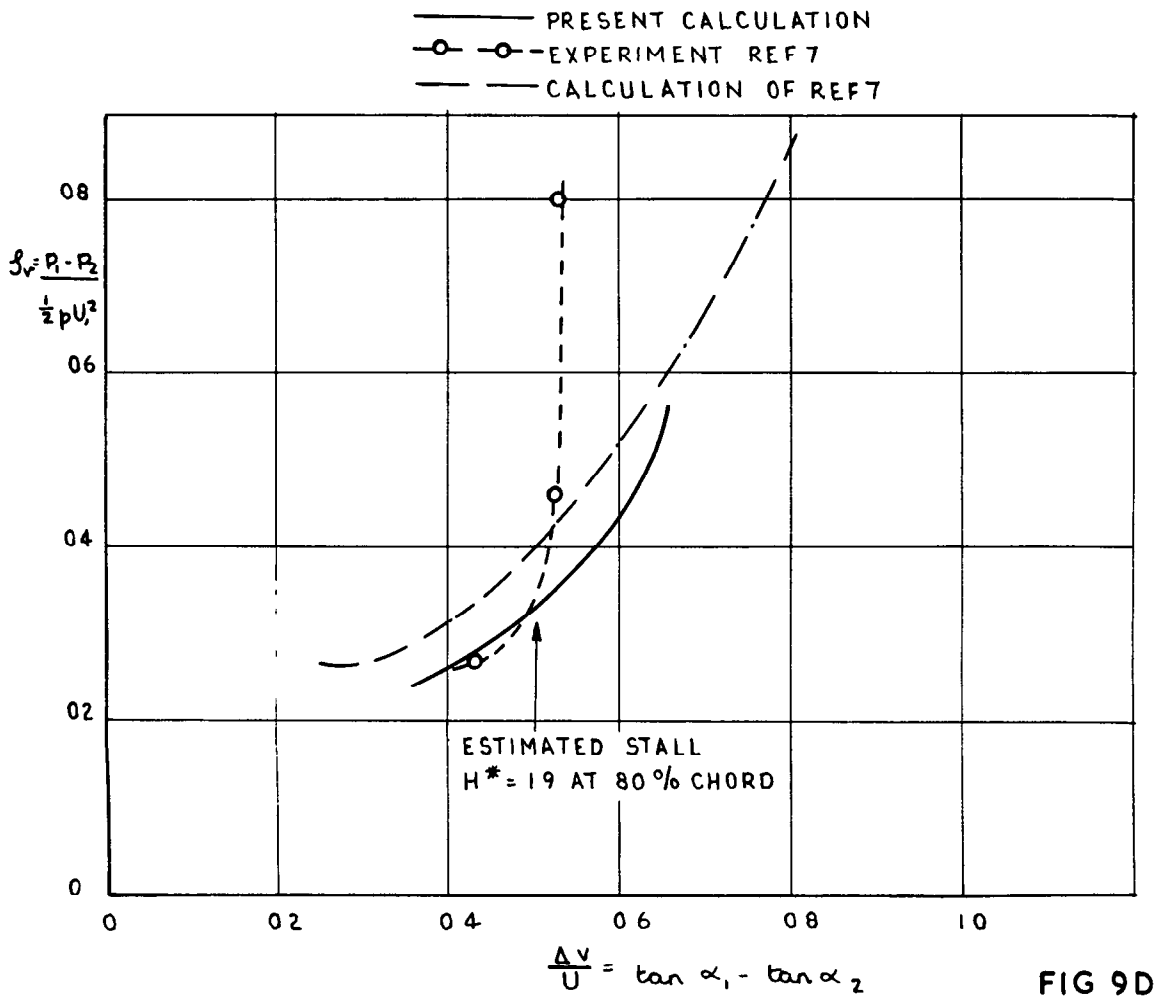

FIG 9D

EXPERIMENTAL AND CALCULATED LIFT DRAG RATIO.

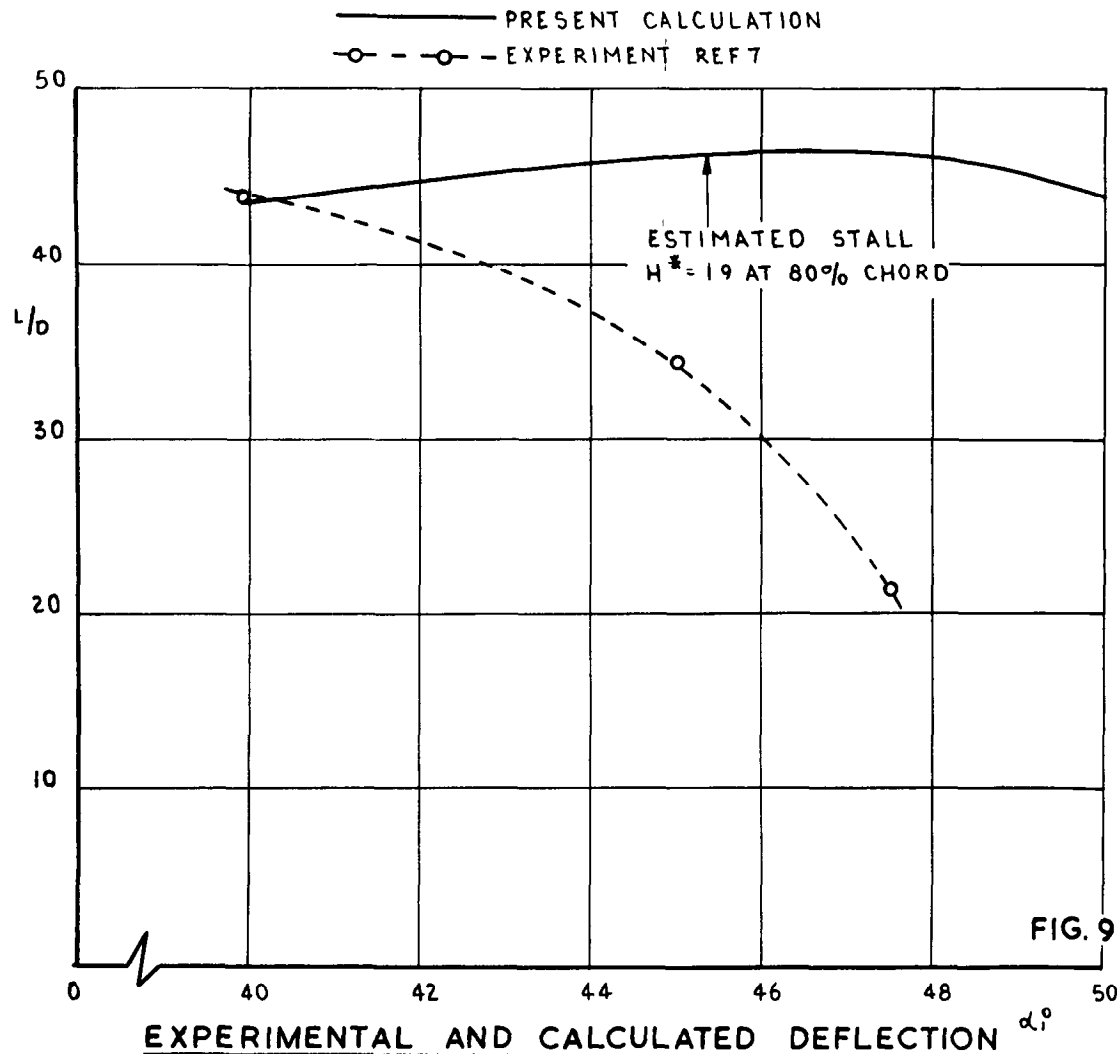

FIG. 9E

EXPERIMENTAL AND CALCULATED DEFLECTION

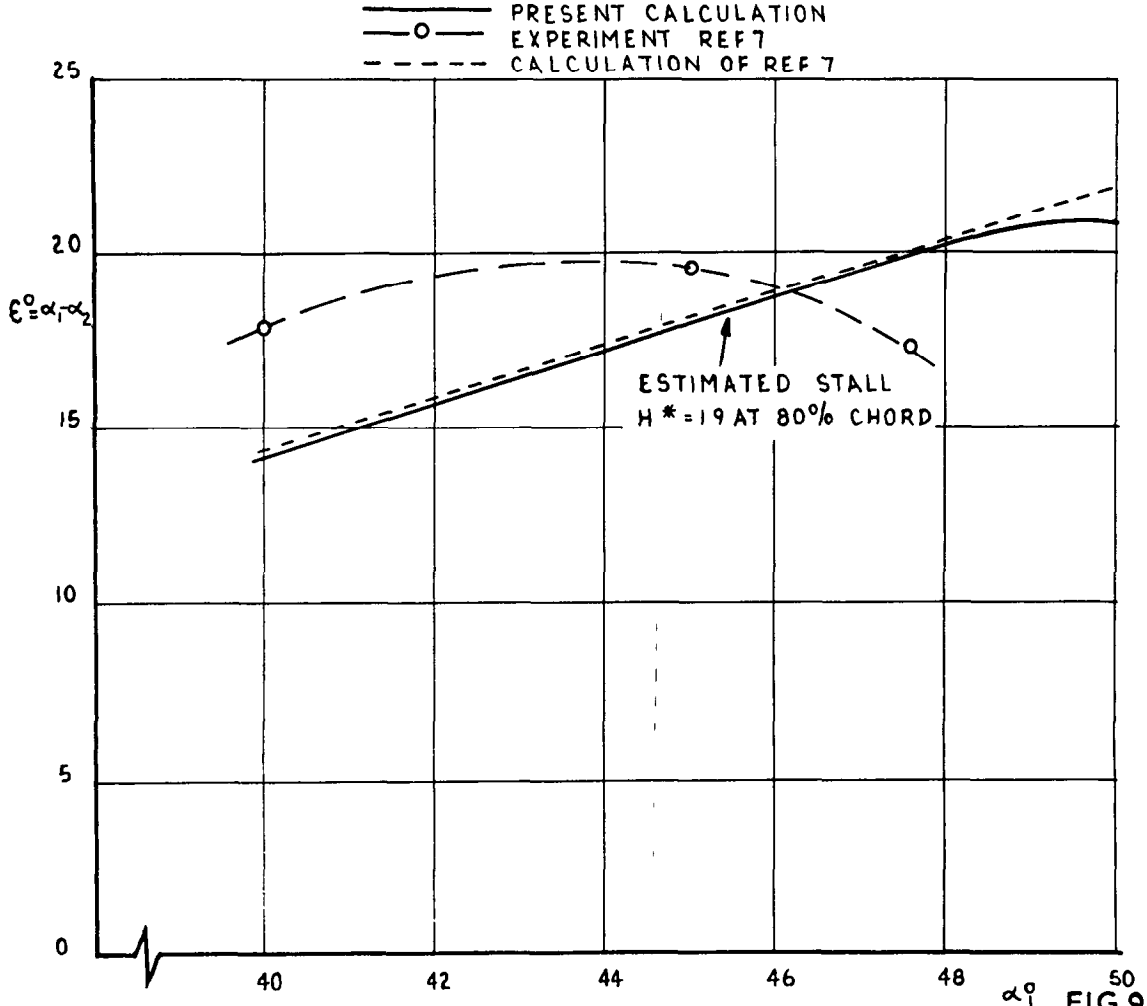

FIG 9F

Printed and published by

HER MAJESTY'S STATIONERY OFFICE

To be purchased from
49 High Holborn, London W C 1
423 Oxford Street, London W 1
13A Castle Street, Edinburgh 2
109 St Mary Street, Cardiff
Brazennose Street, Manchester 2
50 Fairfax Street, Bristol 1
35 Smallbrook, Ringway, Birmingham 5
80 Chichester Street, Belfast 1
or through any bookseller

Printed in England

S.O. Code No. 23 - 9016 - 70